Structural characterization of cobalt(III), nickel(II), copper(II) and iron(III) complexes of tetraazamacrocycles with N-carboxymethyl arms

Judite Costa,[ab] Rita Delgado,[ac] Michael G. B. Drew,[d] Vitor Félix,[ae] Rui T. Henriques[ce] and João C. Waerenborgh[e]

[a] Instituto de Tecnologia Química e Biológica, UNL, Apartado 127, 2781–901 Oeiras, Portugal
[b] Faculdade de Farmácia de Lisboa, Av. das Forças Armadas, 1600 Lisboa, Portugal
[c] Instituto Superior Técnico, Av. Rovisco Pais, 1049–001 Lisboa, Portugal
[d] Department of Chemistry, University of Reading, Whiteknights, Reading, UK RG6 6AD
[e] Dep. Química, Universidade de Aveiro, Campus de Santiago, 3800 Aveiro, Portugal; Instituto Tecnológico e Nuclear, Dep. Química, 2686–953 Sacavém, Portugal

The single crystal structures of complexes $[CoL^1]Br_{0.5}\cdot[NO_3]_{0.5}\cdot5H_2O$ **1**, $[Ni(HL^1)]Br\cdot4H_2O$ **2**, $Ca[CuL^3]NO_3\cdot CH_3CN\cdot2H_2O$ **3** and $[CoL^3]\cdot2H_2O$ **4** were determined, where H_2L^1 is 3,11-bis(carboxymethyl)-7-methyl-3,7,11,17-tetraazabicyclo[11.3.1]heptadeca-1(17),13,15-triene and H_3L^3 is 3,7,11-tris(carboxymethyl)-3,7,11,17-tetraaza-bicyclo[11.3.1]heptadeca-1(17),13,15-triene. In all these complexes the metal centre is encapsulated by the macrocycle in a distorted octahedral environment, the four nitrogen atoms of the tetraaza ring defining the equatorial planes. In the complexes of H_2L^1 the axial positions are occupied by the two carboxymethyl groups which are adjacent to the pyridine ring, while in the complexes of H_3L^3 one of these positions is occupied by one of the carboxymethyl arms adjacent to the pyridine ring and the other by the group opposite to the pyridine moiety. The remaining carboxymethyl arm adjacent to the pyridine ring is further away from the metal centre and plays an important role in the crystal structures of both complexes. Crystals of **3** display a three-dimensional polymeric structure derived from the Ca–O bonds. In the lattice the Ca^{2+} ions are surrounded by eight oxygen atoms, with two calcium ions bridged by two oxygen atoms of carboxylate groups bonded to the copper centres. This large spherical molecule has a centrosymmetric structure with the centre of the core, Ca_2O_2, localised on a crystallographic inversion centre. Additionally, the complexes of H_3L^3 (**3** and **4**) have interesting superstructures based on several $C{=}O\cdots HO$ hydrogen interactions between the carboxylate pendant arms and water molecules. The Fe^{3+} complexes of H_2L^2 (3,11-bis(carboxymethyl)-3,7,11,17-tetraazabicyclo[11.3.1]heptadeca-1(17),13,15-triene) and of H_3L^3 were characterised by EPR and Mössbauer spectroscopy. Both techniques revealed that the complexes of the bis(carboxymethyl) derivative appear as an equilibrium of high- and low-spin state species, the relative amount of the latter increasing with decrease of temperature, and that the complex of the tris(carboxymethyl) derivative appears practically as a high-spin state species. Molecular mechanics studies have provided data to explain the different behaviour of the iron(III) complexes of both ligands.

Introduction

The iron(III) complex of H_2L^1 has been studied by EPR spectroscopy and its magnetic susceptibility determined in the solid state, in the temperature range 3 to 292 K.[1] It was found that all the EPR spectra in frozen solution exhibit two signals, one characteristic of a rhombic iron(III) complex in the low-spin state and the others ascribed to two high-spin iron(III) species with different rhombic distortions. The intensity of the two types of signals decreases with increase of temperature. From the temperature-dependent static susceptibility a magnetic moment of 3.58 μ_B at 292 K was calculated, which remains constant down to 100 K, but below this temperature decreases steeply, exhibiting a value of 1.70 μ_B at 3.1 K. The two experiments were controversial because the proportion of the low-spin species evaluated by the signals of the EPR experiments led to an almost constant value of 35 ± 5%, while the magnetic susceptibility studies pointed out to a continuous increase of the low-spin species with decrease of temperature.[1]

To clarify these results we have synthesized two other similar ligands, H_2L^2 and H_3L^3.[2] EPR and Mössbauer experiments with the iron(III) complexes of both ligands were carried out in a large range of temperatures. Knowledge of the structure
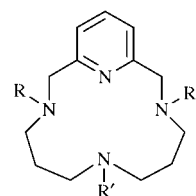
H_2L^1 R = R″ = CH₂CO₂H; R′ = CH₃
H_2L^2 R = R″ = CH₂CO₂H; R′ = H
H_3L^3 R = R′ = R″ = CH₂CO₂H
L^4 R′ = CH₃; R = R″ = pyridylmethyl
H_2L^5 R = CH₃; R′ = R″ = CH₂CO₂H

adopted by those iron(III) complexes should be helpful for understanding these magnetic and spectroscopic features, however in spite of our best efforts to obtain single crystals suitable for X-ray diffraction determinations of the three iron(III) complexes we were not successful. Nevertheless we have obtained good crystals of complexes with the same ligands but different metal ions which gave interesting data about their preferred arrangement.

Experimental

Reagents

The ligands (H_2L^1, H_2L^2 and H_3L^3) were synthesized and characterised in our laboratory by previously reported procedures.[1,2] All the chemicals were of reagent grade and used as supplied without further purification.

Synthesis of metal complexes for X-ray diffraction studies

[CoL^1]Br$_{0.5}$[NO$_3$]$_{0.5}$·5H$_2$O. An aqueous solution of 4.99×10^{-2} mol dm^{-3} Co(NO$_3$)$_2$ (1.75 cm^3, 0.087 mmol) was added to a stirred solution of H_2L^1·3HBr (0.089 mmol) dissolved in the minimum volume of water (≈ 2 cm^3) and the pH increased to 6 by addition of KOH. The mixture was kept overnight at 45 °C and then concentrated to dryness. The residue was taken up in ethanol, the precipitate formed filtered off and the filtrate again concentrated to dryness, then taken up in ethanol and left to stand at 19 °C. Orange crystals suitable for X-ray diffraction studies were formed in ten months. Yield: 70%.

[Ni(HL^1)]Br·4H$_2$O. An aqueous solution of 4.79×10^{-2} mol dm^{-3} Ni(ClO$_4$)$_2$ (1.6 cm^3, 0.076 mmol) was added to a stirred solution of H_2L^1·3HBr (0.080 mmol) dissolved in the minimum volume of water (≈ 2 cm^3) and the pH increased to 3.0 by addition of KOH. The mixture was kept for 4 h at 40 °C and then concentrated to dryness. The residue was taken up in ethanol, the precipitate formed filtered off and the filtrate again concentrated to dryness, then taken up in ethanol–acetonitrile (1:9) and left to stand at 19 °C. One single violet crystal was formed in 45 d.

Ca[CuL^3]NO$_3$·CH$_3$CN·2H$_2$O. The salt Cu(ClO$_4$)$_2$·6H$_2$O (0.019 g, 0.052 mmol) was added to a stirred aqueous solution of [H$_5$L^3][NO$_3$]$_2$ (0.052 mmol), the pH increased to 6 by addition of KOH and then Ca(NO$_3$)$_2$·4H$_2$O (0.05 mmol, 0.012 g) added. The mixture was kept 3 h at 50 °C and then concentrated to dryness. The residue was taken up in ethanol and the inorganic salts formed were filtered off. Then the filtrate was concentrated to dryness, taken up in methanol–acetonitrile (1:1) and left to stand at 19 °C. One single turquoise blue crystal was formed in two months.

[CoL^3]·2H$_2$O. An aqueous solution of 4.99×10^{-2} mol dm^{-3} Co(NO$_3$)$_2$ (0.5 cm^3, 0.025 mmol) was added to a stirred aqueous solution of H_3L^3 (0.026 mmol) and the pH increased to 6.2 by addition of KOH. The mixture was kept for 2 h at 45 °C and then concentrated to dryness. The residue was taken up in ethanol, the precipitate formed filtered off and the filtrate again concentrated to dryness, then taken up in ethanol–acetonitrile (2:1) and left to stand at 19 °C. Red cherry crystals were developed in ten weeks. Yield: 85%.

Synthesis of the Fe^{3+} complexes for EPR and Mössbauer spectroscopic studies

[FeL^2]NO$_3$. The compound Fe(OH)$_3$ was freshly prepared by the addition of 0.1 mol dm^{-3} KOH to a solution of Fe(NO$_3$)$_3$ (0.111 mmol). The precipitate was centrifuged and added to an aqueous solution of H_2L^2 (0.111 mmol). The mixture was heated for about 2 h at 50 °C and left to stand overnight at room temperature. The solution was then concentrated and diethyl ether added to the residue. An orange precipitate was obtained which was dried under vacuum. Yield: 87%. Found: C, 42.1; H, 5.4; N, 14.3. Calculated for C$_{17}$H$_{24}$FeN$_5$O$_7$·H$_2$O: C, 42.2, H, 5.1, N, 14.5%.

[FeL^3]. This complex was prepared by a similar procedure using 0.157 mmol of Fe(OH)$_3$ and the same amount of H_3L^3. Yield: 80%. Found: C, 49.7; H, 5.3; N, 12.5. Calculated for C$_{19}$H$_{25}$FeN$_4$O$_6$: C, 49.5, H, 5.5, N, 12.2%.

Spectroscopic studies

EPR Spectroscopy measurements were made with a Bruker ESP 380 spectrometer equipped with continuous-flow cryostat for liquid helium, operating at X-band. The spectra of the iron(III) complexes were prepared by dissolution of the synthesized compounds in 1.0 mol dm^{-3} NaClO$_4$.

^{57}Fe Mössbauer measurements were recorded in transmission mode using a conventional constant acceleration spectrometer and a 25 mCi ^{57}Co source in a rhodium matrix. The velocity scale was calibrated using an α-Fe foil at room temperature. Isomer shift values are given relative to this standard. The samples of the complexes, [FeL^2]NO$_3$ and [FeL^3], were introduced into perspex holders. Spectra were collected with the absorbers between 296 and 9 K. Low-temperature measurements were obtained using a flow cryostat. The spectra were fitted to lorentzian lines using a modified version of the non-linear least-squares fitting method of Stone.[3]

Crystallography

In Table 1 are summarised the pertinent crystallographic data together with refinement details for complexes [CoL^1]Br$_{0.5}$·[NO$_3$]$_{0.5}$·5H$_2$O **1**, [Ni(HL^1)]Br·4H$_2$O **2**, Ca[CuL^3]NO$_3$·CH$_3$CN. 2H$_2$O **3**, and [CoL^3]·2H$_2$O **4**, respectively. Crystal data for all complexes were collected at 298 K using graphite-monochromated Mo-Kα radiation on a MAR research image plate system ($\lambda = 0.71073$ Å) at Reading University. The crystals were positioned at 70 mm from the image plate; 95 frames were measured at 2° intervals with a counting time suitable for the diffraction pattern exhibited by the complex under investigation. Data analysis was performed with the XDS program.[4]

An empirical absorption correction was applied to the intensities of complexes **2** and **3** using a version of the DIFABS program,[5] modified for the image plate system. Intensities of complexes **1** and **4** were not corrected for absorption effects.

The structures were solved by a combination of direct methods and Fourier-difference syntheses. Hydrogen atoms bonded to the carbon atoms were included in the refinement at geometric positions with C–H default distances. Hydrogen atoms on the water solvent molecules of all four complexes were discernible from Fourier-difference maps and included in the refinement with geometric restraints on O–H and H···H distances consistent with the expected tetrahedral geometry of the water molecule.

The earlier Fourier-difference maps calculated for complex **1** revealed that the Br$^-$ was disordered in the unit cell over four alternative positions. Therefore, this anion was introduced in the refinement on these four positions. For the two positions with more statistical significance an occupation factor of 0.40 was ascribed while for the two remaining positions an occupation factor of 0.10 was included.

Analysis of thermal parameters of complex **2** has shown that the carbon atom bonded to the nitrogen opposite to the pyridine ring had high values in one direction, suggesting that it was affected by some positional disorder. After many trial refinements we found that the following disorder model gave the best fit to the electron density map. Carbon atoms of two methylenic groups of the macrocyclic backbone and the carbon atom of the N-methyl group, accompanied by their hydrogen atoms, were positioned on two alternative positions with refined occupancies leading to two slightly different conformations for the macrocyclic ligand (see below). A refined value of 0.56(2) was obtained for the major disorder component. Two alternative positions with equal probability were also considered for a water solvent molecule of this complex.

All non-hydrogen atoms of the four complexes were refined with anisotropic thermal parameters apart from those affected to some extent by positional disorder, which were refined with isotropic thermal parameters. All hydrogen atoms were refined with isotropic thermal parameters equal to 1.2 times those of

Table 1 Room temperature crystal data and refinement details for metal complexes **1**, **2**, **3** and **4**

	1	2	3	4
Empirical formula	$C_{18}H_{31}Br_{0.5}CoN_{4.5}O_8$	$C_{18}H_{34}BrN_4NiO_8$	$C_{21}H_{32}CaCuN_6O_{11}$	$C_{19}H_{29}CoN_4O_8$
M	537.36	573.11	647.15	500.39
Crystal system	Triclinic^a	Monoclinic	Monoclinic	Monoclinic
Space group	$P\bar{1}$	$P2_1/n$	$P2_1/n$	$P2_1/n$
$a/\text{Å}$	9.635(11)	11.966(12)	8.643(11)	9.889(12)
$b/\text{Å}$	12.653(14)	14.529(17)	18.983(20)	17.524(20)
$c/\text{Å}$	18.080(20)	14.196(16)	17.090(20)	12.398(15)
$a/°$	90.310(10)			
$\beta/°$	93.818(10)	93.01(1)	103.49(1)	97.30(1)
$\gamma/°$	90.003(1)			
$V/\text{Å}^3$	2199(4)	2465(5)	2727(6)	2131(4)
Z	4	4	4	4
$D_c/\text{g cm}^{-3}$	1.623	1.545	1.579	1.560
μ/mm^{-1}	1.743	2.457	1.022	0.861
Reflections measured	7044	7441	9363	5912
Unique reflections	7044	4300 ($R_{int} = 0.0672$)	5019 ($R_{int} = 0.1020$)	3244 ($R_{int} = 0.0244$)
R and R' $[I > 2\sigma(I)]$	0.0737, 0.1997	0.0965, 0.2628	0.0910, 0.1455	0.0390, 0.0963
(all data)	0.1060, 0.2226	0.1350, 0.2946	0.1644, 0.1701	0.0516, 0.1029

^{a} The monoclinic system was also considered, but the R_{int} of 0.6064 obtained when the *hkl* data were merged in the Laue symmetry group $2/m$ unequivocally indicates that this symmetry is not present.

the atoms to which they were bonded. The structures were refined by least-squares method against F^2 until the desired convergence was achieved.

All calculations to solve and refine the structures were carried out with SHELXS and SHELXL within the SHELX 97 package.[6] The molecular and crystal packing diagrams were drawn with the graphical interfaces XPMA and ZORTEP,[7] PLATON[8] and CERIUS 2.[9]

CCDC reference number 186/1585.

See http://www.rsc.org/suppdata/dt/1999/3253/ for crystallographic files in .cif format.

Molecular mechanics calculations

Molecular mechanics calculations were carried out using the Universal Force Field[10] within the CERIUS 2 software.[9] Default parameters were used apart from the terms involving the metal centre. In all conformers investigated the unstrained metal environment was considered to be an ideal geometry. The angle bending terms at the metal centre for octahedral and square pyramidal geometries were restrained to 90 or 180° using a cosine periodic expansion term, since this algorithm incorporates the possibility of one more ideal angle, *e.g.* 90 or 180° for an octahedral geometry. For the bipyramidal geometry those angles were treated individually, using a cosine Fourier expansion term with the angles L_{ax}–M–L_{ax}, L_{eq}–M–L_{eq} and L_{ax}–M–L_{eq} restrained to 180, 120 and 90°, respectively.

The strain energies for different conformers were calculated using a procedure similar to that described before.[2] All M–L bond lengths were fixed at the same value using large force constants for the stretching terms. Then the energy profiles of the conformers relative to M–L distances were obtained by changing those distances successively at 0.05 Å intervals over the range 1.7 to 2.5 Å. Charges were not used because they were difficult to calculate accurately and only have marginal impact on relative strain energies.

The starting coordinates for geometric isomers were obtained from the X-ray determinations or alternatively by manipulation of the coordinates of metal complexes where the macrocyclic ligand is co-ordinated to the metal centre in a geometric arrangement similar to the present ones. Therefore, all six-co-ordinate folded conformers for [ML^1] and [ML^3] were derived from the *cis*-octahedral complex [NiL^4]$^{2+}$ [L^4 = 3,11-bis-(2-pyridylmethyl)-3,7,11,17-tetraazabicyclo[11.3.1]heptadeca-1(17),13,15-triene],[11] the *trans*-octahedral conformers for [ML^1] and [ML^3] from [CoL^1]$^+$ and [CoL^3] and the folded five-co-ordinated conformers from [Cu(H$_2$L^1)Cl]$^+$.[12]

Results

X-Ray diffraction studies

The crystal structures of macrocyclic complexes [CoL^1]-Br$_{0.5}$·[NO$_3$]$_{0.5}$·5H$_2$O **1**, [Ni(HL^1)]Br·4H$_2$O **2**, Ca[CuL^3]NO$_3$·CH$_3$CN·2H$_2$O **3**, and [CoL^3]·2H$_2$O **4** were determined by single crystal X-ray diffraction.

The unit cell of the complex **1** is built up from an asymmetric unit composed by two [CoL^1]$^+$, one Br$^-$, one NO$_3^-$, and five water molecules leading to the molecular formula given. In the crystal lattice the bromine anion is disordered over four positions. The values of the bond lengths and angles found for both cations are identical within the standard limits. Therefore in the present discussion the average values for these structural parameters will be used, unless otherwise stated. The asymmetric unit of **2** consists of one [Ni(HL^1)]$^+$, one Br$^-$ and four crystallisation water molecules. One of the water molecules is disordered over two positions in the crystal lattice. The complex cation presents also some disorder at the level of the macrocyclic backbone and the N-methyl group as described in the Experimental section. Complex **3** is built up from an asymmetric unit composed by one Ca^{2+}, two anions, [CuL^3]$^-$ and NO$_3^-$, and three solvent crystallisation molecules, one acetonitrile and two waters, leading to the molecular formula Ca-[CuL^3]NO$_3$·CH$_3$CN·2H$_2$O. The chemical identity of the cation was investigated carefully considering in refinement Ca^{2+}, K$^+$ or Cu^{2+}. The comparison of R and R' values obtained for Ca^{2+} [0.0910, 0.1455], K$^+$ [0.0930, 0.1841] and Cu^{2+} [0.1341, 0.2821] indicates that calcium is present in the crystal structure, an interpretation which is consistent with the structural environment of the cation, as the distances between the calcium and oxygen atoms are typical of Ca–O bonds. The asymmetric unit of complex **4** comprises one discrete molecule [CoL^3] and two crystallisation water molecules.

Molecular structures of the transition metal complexes

Molecular diagrams including the corresponding atomic notation schemes are shown in Figs. 1 and 2 for complexes of L^1, [CoL^1]$^+$ **1**$^+$ and [Ni(HL^1)]$^+$ **2**$^+$, and in Figs. 3 and 4 for complexes of L^3, [CuL^3]$^-$ **3**$^-$ and [CoL^3] **4**. The disorder model found for the macrocyclic backbone in cation **2** leads to two different conformational isomers in the solid state. Therefore, in Fig. 2 is shown the macrocyclic conformation and the N-methyl position with major occupation factors in the unit cell. Furthermore the charge balance requires protonation of the complex cation, which probably occurs on one of the free
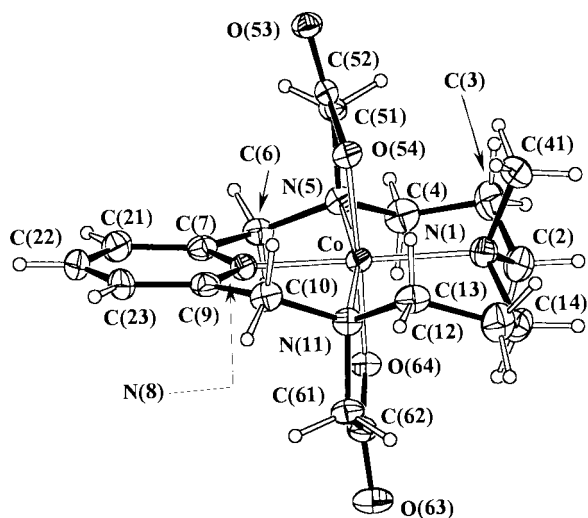
Fig. 1 The molecular structure of [CoL¹]⁺ **1**⁺ with the labelling scheme adopted. Ellipsoids are drawn at 30% probability level for all structures.
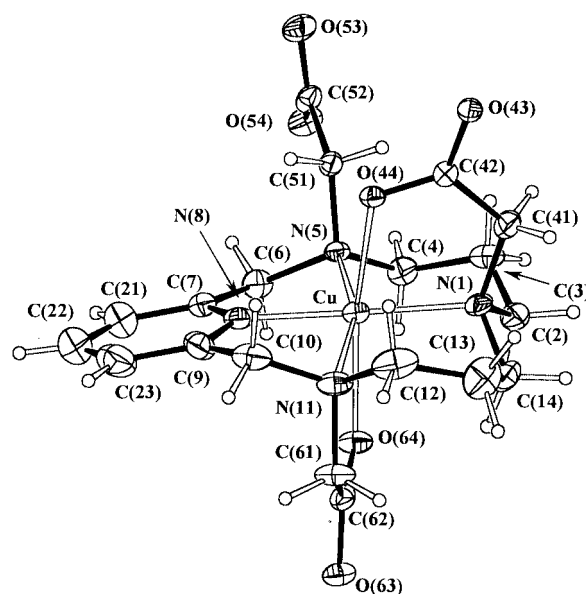

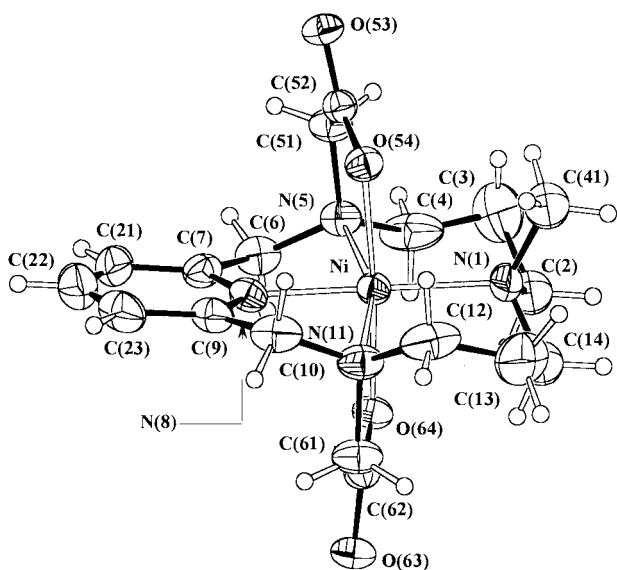**Fig. 2** The molecular structure of [Ni(HL¹)]⁺ **2**⁺ with the labelling scheme adopted.

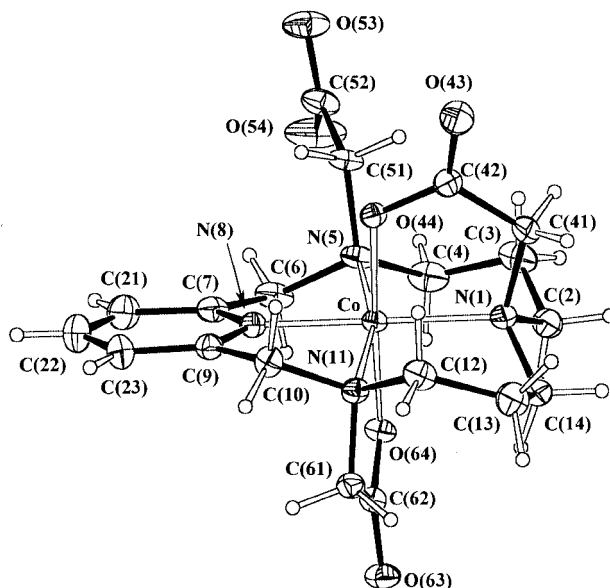**Fig. 3** The molecular structure of [CuL³]⁻ **3**⁻ with the labelling scheme adopted.

Fig. 4 Molecular structure of [CoL³] **4** with the labelling scheme adopted.

oxygen atoms of two carboxylate groups. However this hydrogen was not localised from the Fourier-difference maps and consequently not included in the structure refinement or in Fig. 2.

Selected bond lengths and angles are given in the Table 2 for the four complexes. In all of them the metal centre is encapsulated by the macrocycle in a distorted octahedral environment. The four nitrogen atoms of the tetraaza ring define the equatorial planes. The six-co-ordination is completed with two oxygen atoms of the appended carboxylate groups. However, the complexes of H₂L¹ and H₃L³ exhibit different stereochemistries. In the complexes of H₂L¹ the axial octahedral positions are occupied by two carboxylate groups, which are adjacent to the pyridine ring. In contrast, in complexes of H₃L³ one of these positions is occupied by one of the carboxylate arms adjacent to the pyridine ring and the other by the carboxylate group opposite to the pyridine moiety. The remaining carboxymethyl arm adjacent to the pyridine ring is further away from the metal centre leading to distances between the oxygen atom O(54) and the metal centre of 5.000(6) and 4.988(5) Å in **3** and **4**, respectively. This free arm plays an important role in the crystal structures of both complexes (see below).

The structural parameters associated with the metal co-

ordination sphere show a distorted octahedral geometry for all complexes. However, the angles at the metal centres are close to the expected values of 90 and 180° of an ideal octahedral geometry. The highest deviation from ideal octahedral angles is in the equatorial plane for the angle N(11)–M–N(5). The best least-squares plane through the nitrogen atoms shows a very small tetrahedral distortion indicating that these atoms are very close to planarity [± 0.009(5) Å for **1**, ± 0.006(4) Å for **2**, ± 0.052(26) Å for **3** and ± 0.040(1) Å for **4**]. The metal ions are on the N₄ co-ordination plane. These structural features suggest that in all these complexes there is a good match between the size of the macrocyclic cavity and that of the metal ion.

Furthermore the endocyclic torsion angles listed in Table 3 indicate that the macrocyclic backbone has the same conformation in complexes **1**, **3** and **4** and that the macrocycle provides a cavity of sufficient size to accommodate metals, such as Niᴵᴵ, Coᴵᴵᴵ or Cuᴵᴵ. In other words any steric strain imposed by the stereochemical demands of the metal might change considerably the values of these torsion angles. The torsion angles listed for complex **2** differ slightly from those found for the other three complexes, but this is due to the disorder found in the

Table 2 Selected bond lengths (Å) and angles (°) in the transition metal co-ordination sphere of complexes **1**, **2**, **3** and **4**

	1 [M = Co^{III} and $x = 54$]	**2** [M = Ni^{II} and $x = 54$]	**3** [M = Cu^{II} and $x = 44$]	**4** [M = Co^{III} and $x = 44$]
Axial				
M–O(x)	1.892(4)	2.095(5)	2.369(4)	1.887(3)
M–O(64)	1.891(4)	2.090(5)	2.279(5)	1.895(3)
O(64)–M–O(x)	177.6(2)	175.2(2)	164.4(2)	176.0(1)
Equatorial				
M–N(1)	2.043(5)	2.077(7)	2.051(6)	2.000(2)
M–N(5)	2.002(5)	2.114(7)	2.140(5)	2.071(2)
M–N(11)	1.988(5)	2.116(8)	2.137(6)	2.005(3)
M–N(8)	1.882(5)	1.972(7)	1.949(6)	1.884(3)
N(8)–M–N(1)	178.9(2)	178.9(4)	178.5(2)	177.7(1)
N(5)–M–N(1)	97.8(2)	100.9(4)	99.4(2)	99.9(1)
N(11)–M–N(1)	96.6(2)	98.9(4)	98.8(2)	96.1(1)
N(8)–M–N(5)	82.9(2)	80.1(3)	81.2(2)	82.0(1)
N(11)–M–N(5)	165.5(2)	160.1(3)	161.4(2)	163.7(1)
N(8)–M–N(11)	82.6(2)	80.0(3)	80.8(3)	82.1(1)

macrocyclic ligand instead of other steric strain created by the nickel(II) centre. Table 3 includes the torsion angles found for the related complex [CuL^2] **5** (see below)[2] and shows the same conformation as in the present complexes.

Among these structurally characterised complexes, **3** exhibits the strongest octahedral distortion. As would be expected for a copper(II) complex, the axial Cu–O bond lengths are longer than the equatorial Cu–N bond lengths, which is due to the Jahn–Teller effect.[13] The axial Cu–O bond lengths [2.279(5) and 2.369(4) Å] are similar to those found for the complex [CuL^2] **5** [2.300(5) and 2.320(6) Å], which displays also an elongated distorted CuN$_4$O$_2$ octahedral co-ordination sphere.[2] The compound H$_2$L^2 has the same macrocyclic backbone as H$_2$L^1 or H$_3$L^3 but the ligands differ in the substituent in the nitrogen *trans* to the pyridine ring. However, the axial angle between the copper centre and the carboxymethyl arms adjacent to the pyridine ring reported for **5**, of 178.3(2)°, reveals less axial distortion than found for **3**, where the axial O–Cu–O angle is only 164.4(2)°. Therefore, this comparison suggests that the axial O–Cu–O angle is determined by the longer axial Cu–O bond lengths as well as by the relative position of the arms on the macrocyclic backbone. In other words the association in complex **3** of these two structural features prevents the oxygen atoms of the carboxymethyl groups achieving the ideal axial positions of an octahedron leading to an axial angle O–Cu–O smaller than the expected value of 180°. In contrast, the remaining three complexes have shorter axial M–O distances [average values: Co^{III}–O 1.892(4) Å for **1**, Ni^{II}–O 2.092(5) Å for **2** and Co^{III}–O 1.891(3) Å for **4**] the corresponding axial O–M–O angles being close to the ideal value [177.6(2)° for **1**, 175.2(2)° for **2** and 176.0(1)° for **4**].

A crystal structure determination is reported for a copper complex of H$_2$L^1, [Cu(H$_2$L^1)Cl]$^+$,[12] where the co-ordination geometry of the copper centre is approximately trigonal bipyramidal, the equatorial plane being defined by the nitrogen atoms adjacent to the pyridine ring and the oxygen of one carboxylate arm. The axial positions are occupied by the nitrogen atom of the pyridine ring and by a chloride. The remaining carboxymethyl group and the nitrogen *trans* to the pyridine ring are protonated and consequently not co-ordinated. Therefore, the different protonation state of this complex from that studied in this work prevents a direct comparison of their structures. However, it is apparent from the structure of [Cu(H$_2$-L^1)Cl]$^+$ that the longer Cu-O bond length [2.59(2) Å] has also a crucial relevance for the distortion reported for this complex, namely on the angles at the copper centre.[12]
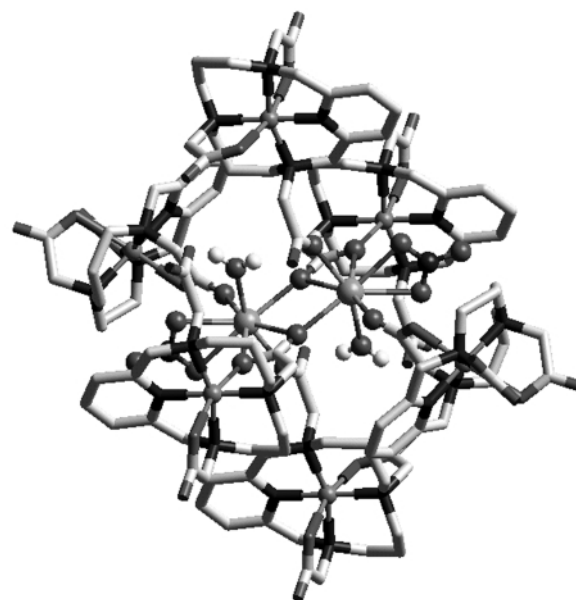

Fig. 5 The building unit in the solid state of the 3-D polymeric structure of the compound Ca[CuL^3]NO$_3$·CH$_3$CN·2H$_2$O **3**. The hydrogen atoms are omitted for clarity except for those of the water molecules bonded to the Ca^{2+} centres. The macrocyclic framework is represented in the cylinder mode and the co-ordination spheres of the Ca^{2+} and the Cu^{2+} centres are drawn in the ball and stick mode.

In all four complexes the M–N distance to the pyridine nitrogen is shorter than to the other nitrogen atoms. This bond length pattern is typical of metal complexes with tetraaza-macrocylic compounds containing one pyridine moiety.[2,14]

Crystal structures

An additional detailed study of the crystal structures was carried out. Crystals of complex **3** display a striking three-dimensional polymeric structure resulting from the Ca–O bonds, which are in the range 2.328(5) to 2.630(5) Å. A view of the extended structure of this complex illustrating the co-ordination environment of Ca^{2+} ions is presented in the Fig. 5. In the lattice all Ca^{2+} ions are surrounded by eight oxygen atoms: one from a water molecule, two from a nitrate and five from carboxylate groups of three macrocyclic units [CuL^3]$^-$. Furthermore, two calcium ions are bridged by two oxygen atoms of carboxymethyl groups bonded to the copper centres leading to a Ca···Ca distance of 4.129(5) Å and an angle Ca–O–Ca of 112.4(2)°. This large spherical molecule has a centrosymmetric structure with the centre of the core Ca$_2$O$_2$ localised on a crystallographic inversion centre. The molecular dimensions of the Ca^{2+} co-ordination polyhedra listed in Table 4 indicate that the environment of this ion can be described as a distorted triangulated dodecahedron (bisdisphenoid).[15] From the Structural Cambridge Data Base (CSD)[16] we retrieved five structures of calcium complexes having two calcium centres with co-ordination environments of eight oxygen atoms, two of which are bridging ligands between these two ions. The Ca···Ca distances found for **3** are in the range of Ca to Ca intermolecular distances reported for those complexes of 3.864–4.330 Å. The random distribution of Ca–O distances found in **3** made it not possible to establish straightforwardly any relationship between the values of these distances and any particular structural feature present in the calcium(II) polyhedra. However these distances compare well with those reported for the mentioned complexes with CSD refcodes CALMAD, FAHRUB, PIXPUH, RUMPEU and VEXYIG. Acetonitrile and water crystallisation solvent molecules are accommodated in the interstitial positions of the 3-D network of complex **3**.

All the studied complexes contain water molecules and the

Table 3 Selected endocyclic torsion angles (°) in the metal complexes of H_2L^1, H_2L^2 and H_3L^3, *i.e.* **1**, **2**, **3**, **4** and **5**

	Complex	N(8)–C(7)[a]	C(7)–C(6)	C(6)–N(5)	N(5)–C(4)	C(4)–C(3)	C(3)–C(2)	C(2)–N(1)	N(1)–C(14)	C(14)–C(13)	C(13)–C(12)	C(12)–N(11)	N(11)–C(10)	C(10)–C(9)	C(9)–N(8)
1[b]	[CoL¹]⁺	−179.8(5)	−27.2(7)	159.2(5)	−170.7(5)	66.4(8)	−73.0(8)	176.8(6)	174.5(6)	43.0(10)	29.0(10)	−178.4(6)	157.1(5)	−24.0(7)	−175.5(5)
		−177.9(5)	*−29.8(7)*	*161.0(6)*	*−172.1(7)*	*71.8(4)*	*−75.8(4)*	*177.5(8)*	*173.7(5)*	*41.7(9)*	*28.3(9)*	*−180.0(5)*	*158.9(5)*	*−25.6(7)*	*−175.1(5)*
2[b]	[Ni(HL¹)]⁺	−177.6(6)	−34.4(9)	159.1(7)	−168.5(10)	78.1(13)	−87.1(15)	179.6(13)	179.1(13)	50(2)	21.5(19)	−173.1(9)	154.8(7)	−24.1(9)	−175.8(6)
		−177.6(6)	*−34.4(9)*	*159.1(7)*	*−168.5(10)*	*13(2)*	*61(2)*	*174.2(17)*	*179.9(18)*	*−89.8(18)*	*85.5(15)*	*−173.1(9)*	*154.8(7)*	*−24.1(9)*	*−175.8(6)*
3	[CuL³]⁻	−172.5(7)	−20.8(9)	151.3(6)	−168.2(6)	69.4(8)	−73.7(8)	172.6(6)	177.1(7)	49.6(12)	24.4(12)	−171.5(7)	157.8(7)	−33.8(9)	−178.3(6)
4	[CoL²]	−174.0(3)	−28.5(3)	158.0(2)	−168.8(3)	71.8(4)	−72.3(4)	175.2(3)	174.5(3)	38.7(4)	28.8(4)	−179.0(3)	161.1(2)	−27.1(3)	−179.0(2)
5[c]	[CuL²]	−176.3(7)	−24.3(9)	157.5(7)	−163.2(8)	71.7(11)	−75.7(11)	179.2(7)	167.3(7)	45.5(11)	28.64(1.07)	−173.6(7)	158.2(6)	−38.0(8)	−177.2(7)

[a] Bonds denote the central atoms that determine the endocyclic torsion angle started at N(8)–C(7). They are labelled using the numbering scheme shown in Figs. 1, 2, 3 and 4 for the studied complexes. [b] The italic values reported for [CoL¹]⁺ correspond to the second molecule of the asymmetric unit while for [Ni(HL¹)]⁺, these values are relative to the minor component of the disorder present in the crystal lattice. [c] Ref. 2.

intermolecular interactions resulting from the hydrogen bonding between water molecules and carboxymethyl groups obviously play a determinant role in the crystal structures of **1**, **3** and **4**, apart from other hydrogen bonding interactions involving water molecules and other hydrogen acceptors present in the crystals. In **2** only the last type of hydrogen bonding interactions is present in the crystal structure. In Table 5 are listed the intermolecular distances and angles for hydrogen bonding found for the studied complexes.

The metal complexes of H_3L^3 offer interesting superstructures based on several C=O $\cdots$ HO hydrogen interactions between the carboxylate pendant arms and the water molecules. Figs. 6 and 7 show the patterns exhibited by **3** and **4**, respectively. In the lattice of complex **3** two water molecules bridge the deprotonated carboxylate arms of two $[CuL^3]^-$ complex units with formation of centrosymmetric twelve-membered ring systems (four OH $\cdots$ O=C distances, two 2.22 and two 2.29 Å, see Fig. 6b). Thus, from the viewpoint of the hydrogen bonding interactions these two complex units form formally a supra-anionic centrosymmetric structure. Furthermore the second independent water molecule interacts concomitantly with free (OH $\cdots$ O=C 2.43 Å) and co-ordinated carboxymethyl arms (OH $\cdots$ O=C 2.10 Å) of $[Cu(L^3)]^-$ leading to a 3-D polymeric structure based only on hydrogen bonds. No other hydrogen bonding interactions involving the nitrate groups and water molecules were found, but a detailed analysis reveals that intermolecular interactions between the pyridine ring and this anion occur *via* short C–H$^{\delta+}\cdots$O$^{\delta-}$ hydrogen bonds of 2.31 Å

with a C–H$^+\cdots$O$^-$ angle of 151.0°. In conclusion the crystalline structure of complex **3** displays two connectivities: one based on OH $\cdots$ O hydrogen bonds and another derived from Ca–O bonds.

In the crystalline structure of **4** two complex units also interact *via* OH $\cdots$ O hydrogen bonds between the oxygen atoms of the free deprotonated carboxymethyl arms and water bridges (four OH $\cdots$ O=C distances, two of 1.97 and two of 1.96 Å, respectively). The water bridges are formed by two water molecules with OH $\cdots$ O distances of 1.98 Å. As in **3**, the interaction between these structural moieties results in large centrosymmetric ring systems, now with sixteen members (see Fig. 7b). The superstructures are then linked to four complex units of neighbouring superstructures *via* OH $\cdots$ O hydrogen bonds leading to a polymeric structure for the crystal (see Fig. 7a). These interactions involve a water molecule and oxygen atoms of the carboxymethyl groups bonded to the metal centre, the distances OH $\cdots$ O=C being 2.06 Å.

The crystal packing for complex **1** shown in Fig. 8 reveals that the asymmetric unit is composed by two molecules of $[CoL^1]^+$, which have different environments in the crystal. One complex cation is not involved in other significant intermolecular interactions while the other participates in hydrogen bonding interactions with crystallisation water molecules *via* one oxygen atom of its carboxylate groups. Four water molecules are connected *via* hydrogen bonding in a centrosymmetric arrangement forming an eight-membered ring system with two independent O $\cdots$ HO distances of 2.03 and 2.11 Å, respectively. In addition, hydrogen bonds between the ring and another independent water molecule occur with OH $\cdots$ O distances of 1.95 Å. Layers composed by water ring systems are stacked with layers formed by the metal complex units. The two types of layers are connected *via* water molecules that act as bridges between an oxygen atom of the carboxymethyl arms of the metal complex and a water molecule of the water ring systems. The C=O $\cdots$ HO and O $\cdots$ HO distances are 2.02 and 1.93 Å, respectively. The bridging water molecules form also with the remaining water molecule a short hydrogen bond [O $\cdots$ HO 1.80 Å]. Furthermore the nitrate anions interact with a CH$_2$ of a carboxymethyl arm and with the pyridine ring of the macrocycle *via* short charge assisted C–H$^{\delta+}\cdots$O$^{\delta-}$ inter-

Table 4 Selected distances (Å) and angles (°) in the calcium co-ordinated polyhedra

Ca$\cdots$Ca^i	4.129(5)		
Ca–O(43)	2.529(5)	Ca–O(43^i)	2.438(5)
Ca–O(44)	2.630(5)	Ca–O(54^{iii})	2.379(5)
Ca–O(63^{ii})	2.328(5)	Ca–O(300^{ii})	2.417(5)
Ca–O(101^{ii})	2.534(8)	Ca–O(102^{ii})	2.553(7)
Ca^i–O(43)–Ca	112.4(2)	O(43^i)–Ca–O(43)	67.6(2)

Symmetry operations: i $-x + 1$, $-y$, $-z + 2$; ii $-x + \frac{1}{2}$, $y - \frac{1}{2}$, $-z + \frac{3}{2}$; iii $x + 1$, y, z.

Table 5 Dimensions of the hydrogen bond lengths in the metal complexes **1**, **2**, **3** and **4**

		H$\cdots$A/Å	D$\cdots$A/Å	H$\cdots$A$\cdots$D/°
1	$[CoL^1]Br_{0.5}\cdot[NO_3]_{0.5}\cdot 5H_2O^a$	[A = O; D = O]		
	O(200)–H(201)$\cdots$O(500)	1.95	2.789	169.2
	O(200)–H(202)$\cdots$O(300)	1.93	2.781	178.6
	O(300)–H(301)$\cdots$O(63) $[-x + 1, -y + 1, -z + 1]$	2.02	2.863	172.5
	O(300)–H(302)$\cdots$O(600)	1.80	2.593	154.8
	O(400)–H(401)$\cdots$O(200) $[-x + 1, -y + 1, -z + 2]$	2.11	2.938	163.8
	O(400)–H(402)$\cdots$O(200)	2.03	2.867	169.6
2	$[Ni(HL^1)]Br\cdot 4H_2O^a$	[A = O; D = Br or O]		
	O(200)–H(201)$\cdots$Br $[-x + \frac{5}{2}, y - \frac{1}{2}, -z + \frac{1}{2}]$	2.45	3.276	164.8
	O(200)–H(202)$\cdots$O(300)	2.25	2.814	123.7
	O(300)–H(301)$\cdots$Br	2.57	3.401	167.2
	O(400)–H(401)$\cdots$Br $[-x + \frac{5}{2}, y - \frac{1}{2}, -z + \frac{1}{2}]$	2.60	3.405	158.6
3	$Ca[CuL^3]NO_3\cdot CH_3CN\cdot 2H_2O$	[A = O; D = O]		
	O(300)–H(301)$\cdots$O(53) $[-x + \frac{1}{2}, y + \frac{1}{2}, -z + \frac{3}{2}]$	2.22	2.799	125.4
	O(300)–H(302)$\cdots$O(54) $[x + \frac{1}{2}, -y + \frac{1}{2}, z - \frac{1}{2}]$	2.29	3.103	160.3
	O(400)–H(402)$\cdots$O(53) $[-x - \frac{1}{2}, y + \frac{1}{2}, -z + \frac{3}{2}]$	2.43	3.011	125.8
	O(400)–H(401)$\cdots$O(64)	2.10	2.929	165.3
4	$[CoL^3]\cdot 2H_2O$	[A = O; D = O]		
	O(100)–H(101)$\cdots$O(54) $[-x, -y, -z]$	1.97	2.806	166.9
	O(100)–H(102)$\cdots$O(63)	2.06	2.893	168.5
	O(200)–H(201)$\cdots$O(53)	1.96	2.797	169.3
	O(200)–H(202)$\cdots$O(100) $[x, y, z + 1]$	1.98	2.783	159.4

^{a} The intermolecular interactions involving the disordered species are not all listed: Br in complex **1** and one of the water molecules in **2**.
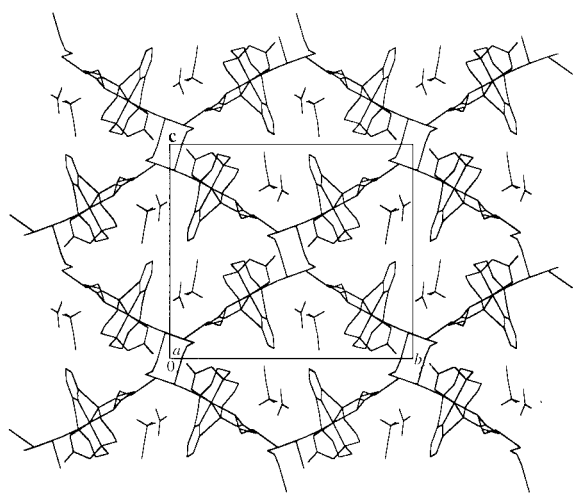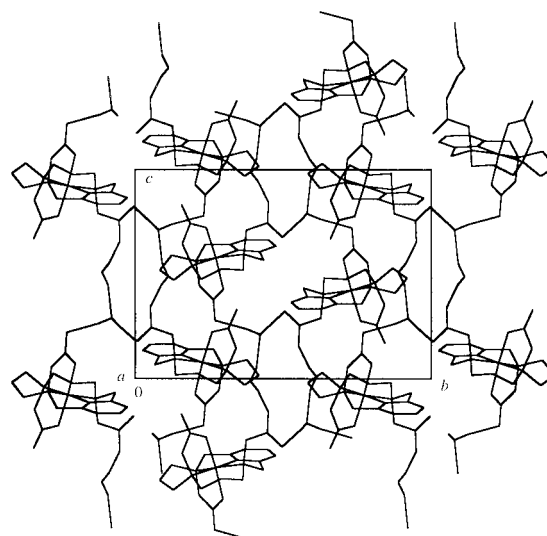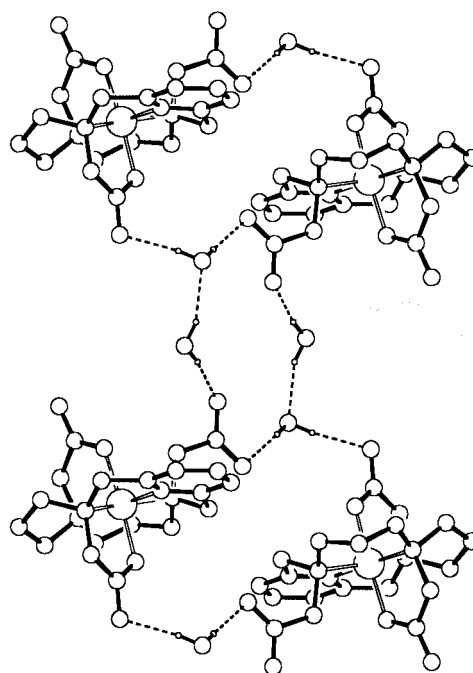
(a)
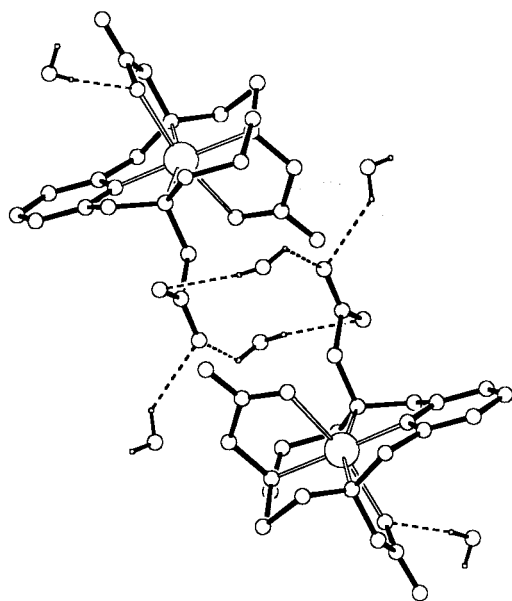
(b)

Fig. 6 Crystal packing for compound Ca[CuL³]NO₃·CH₃CN·2H₂O **3** showing the pattern of hydrogen bond lengths: (a) perspective view perpendicular to the *a* axis, (b) crystallographic motif based on hydrogen bonds. The Ca²⁺ ions are omitted for clarity.

molecular contacts [C sp³–H···O 2.25 Å, 168.5° and C sp²–H···O 2.39 Å, 155.3°]. The intermolecular distances between the bromine and oxygen atoms of water molecules are less than the sum of their van der Waals radii, suggesting that these two species are involved in the hydrogen bonding interactions, but the disorder exhibited by bromine anions prevents a detailed analysis. However, the inclusion of these anions in the crystal packing results in the formation of a three-dimensional network derived from OH···Br interactions with distances O···Br in the range 3.047–3.472 Å.

In contrast with **1**, **3** and **4**, the nickel(II) complex **2** does not reveal other significant intermolecular interactions between the complex cations [Ni(HL¹)]⁺ and the remaining species that comprise the crystal structure, such as the Br⁻ and water molecules. This structural feature probably is due to the protonated state of the macrocyclic ligand in the metal complex. The crystal exhibits zigzag chains composed by water molecules and bromine anions in a 2:1 stoichiometric ratio. The intermolecular interactions in the chains occur obviously *via* OH···O [2.25 Å] and OH···Br [2.45 and 2.57 Å] hydrogen bonds. Additionally the Br⁻ interacts with the third independent molecule present in the crystal, the OH···Br distance

(a)

(b)

Fig. 7 Crystal packing for complex [CoL³]·2H₂O **4** showing the pattern of hydrogen bond lengths: (a) perspective view perpendicular to the *a* axis, (b) crystallographic motif based on hydrogen bonds showing the formation of sixteen-membered ring systems.

being 2.60 Å. The disordered water molecule was not included in the analysis of the hydrogen bonding interactions.

Spectroscopic studies of the Fe³⁺ complexes

The [FeL¹]⁺ complex has been studied by EPR spectroscopy in frozen solutions, as well as by magnetic susceptibility, in the solid state. Both studies were performed in a large range of temperatures, 3 to 292 K.[1] The EPR spectra exhibit two types of signals, one characteristic of a rhombic iron(III) complex in the low-spin state, with resonances at 2.683, 2.337 and 1.721, and the other signals, located at lower field, were assigned to two high-spin iron(III) species having rhombic distortions (E/D) of 0.15 and 0.275, respectively. The determination of the percentage of the low-spin species from the signals of the EPR experiments led to an almost constant value (35 ± 5%) for the
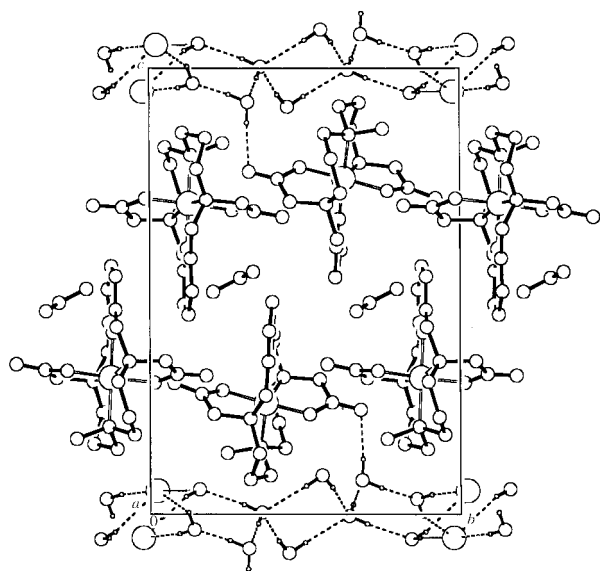
Fig. 8 Perspective view of the crystal packing for compound [CoL¹]·Br₀.₅·[NO₃]₀.₅·5H₂O **1** perpendicular to the *a* axis.

Table 6 Rhombic distances (*E/D*) and effective *g* values expected from the high-spin species of the iron(III) complexes of H₂L² and H₃L³. The values observed in the experimental spectra are italicised.

Complex	*E/D*	Doublet	g_1	g_2	g_3
[FeL²]⁺	0.12	$\|\pm5/2\rangle$	*9.97*	0.09	0.10
		$\|\pm3/2\rangle$	*5.57*	2.41	2.65
		$\|\pm1/2\rangle$	1.60	*8.32*	*3.25*
[FeL³]	0.14	$\|\pm5/2\rangle$	*9.95*	0.12	0.14
		$\|\pm3/2\rangle$	*5.45*	2.69	2.98
		$\|\pm1/2\rangle$	1.49	*8.57*	2.88

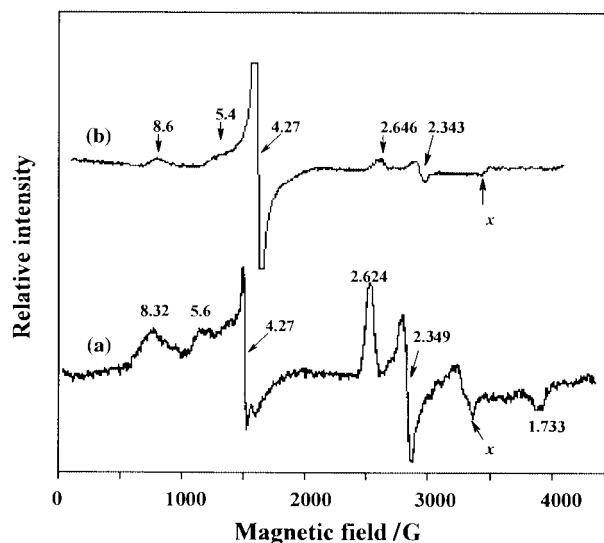**Fig. 9** The X-band EPR spectra of the iron(III) complex of H₂L² at 4 K, (a) and H₃L³ at 10 K (b). Both complexes were prepared in 1.0 mol dm⁻³ NaClO₄. Spectra were recorded at $v = 9.64$ GHz; microwave power 2.4 mW; modulation amplitude 1 mT; *x* is an impurity of the instrument cavity.

range of temperature studied. On the other hand, the temperature-dependent static susceptibility study indicated that the magnetic moment value is almost constant in the region 292 to 100 K (μ_{eff} is 3.58 μ_B at 292 K), but below 100 K it decreases steeply, exhibiting a value of 1.70 μ_B at 3.1 K.[1] It is difficult to reconcile the results obtained by the two techniques unless the later decrease is due to interactions in the solid state.

In the present work we have carried out EPR experiments (X band) in a large range of temperatures with the iron(III) complexes of the other two ligands, [FeL²]⁺ (4 to 200 K) and [FeL³] (10 to 60 K). The spectra of the iron(III) complex of the bis(carboxymethyl) derivative are similar to those of the previously studied complex of H₂L¹,[1] but the spectra recorded for the complex of the tris(carboxymethyl) derivative have a quite different aspect, although the assignment of the resonances of both complexes show more similarities than differences.

The spectra of [FeL²]⁺ exhibit signals at high and low field characteristic of low- and high-spin iron(III) species, respectively, see Fig. 9 (a). The signals at low field, as usual, are not observed at temperatures higher than 120 K, and their multiple structure is only perceptible below 25–30 K, while the high field resonances are observed in the entire range of temperatures. Both the signals increase in intensity with decrease of temperature. The principal resonances of the low-spin species appear at *g* values of 2.624, 2.349 and 1.733. Those corresponding to the high-spin species are observed as large peaks centred at the *g* values of 8.32, 5.6, and the usual resonance of free iron also appears at 4.27 (due to the decrease of the solubility of the complexes with the increase of pH, it was necessary to record the spectra at pH values where small amounts of aqueous iron(III) were expected from speciation diagrams).

The spectra of the iron(III) complex with the tris(carboxymethyl) derivative, [FeL³], exhibit as principal signals those at low field which can be assigned to high-spin species, although at temperatures below 10 K resonances corresponding to a very small amount of a low-spin species also appeared at high field, see Fig. 9 (b). The principal features at low field have also large peaks centred at 8.6, 5.4 and 4.27. The signals of low intensity of the low-spin species appear at *g* values of 2.646, 2.343 and 1.730.

The EPR parameters obtained for both complexes at low field are characteristic of high-spin iron(III) in a rhombically distorted electronic environment described by the spin Hamiltonian $H = g_o\beta\vec{H}\cdot\vec{S} + D[S_z^2 - \frac{1}{3}S(S+1) + (E/D)(S_x^2 - S_y^2)]$ where $S = 5/2$, $g_o = 2.0$, *D* and *E* are the axial and rhombic zero-

field splitting parameters, respectively. The zero-field splitting term in the above equation partly removes the degeneracy of the spin sextet and three Kramer's doublets result.[17,18] If the separation of the doublets is large compared to *βH*, and if the electronic spin relaxation is sufficiently slow, each doublet is expected to give rise to its own resonance, which can be described in terms of an effective $S = 1/2$ spectrum with three effective *g* values, not all observed. The resulting nine *g* values depend on the parameter *E/D*.[17,18] The *g* values obtained for the complexes [FeL²]⁺ and [FeL³] can be fairly well reproduced by the rhombicity parameters, *E/D* = 0.12 and 0.14, while the value found[1] for [FeL¹]⁺ was 0.15.[1] The effective *g* values expected for each Kramers doublet for these values of *E/D* are indicated in Table 6, where the observed resonances in the spectra, Fig. 9, are underlined. As larger values of the rhombicity parameter mean more distorted environments around the metal ion, it is possible to conclude that the three complexes present no significant environment differences, although the most distorted is the previously studied [FeL¹]⁺ followed by [FeL³].

The signals at higher field of both complexes are typical of low-spin d⁵ systems in distorted octahedral environments.[18–22] In general, in this configuration the *g* values are sensitive to small changes in the structure. They can be related to the parameters that describe the electronic ground state of the complex by coefficients *A*, *B* and *C* which are related to the axial distortion, μ, the rhombic distortion parameter, *R*, the energy of the Kramers doublet, E_1, and the spin–orbit coupling constant, λ (see equations below Table 7). Therefore, μ is a measure of the difference in bonding perturbation of the four equatorial and the two axial donor atoms and *R* is a measure of the energy gap between d_{xz} and d_{yz}. The experimental spectra give only the magnitude of the *g* values. To assign those values

Table 7 Spectroscopic EPR data for the Fe^{3+} complexes of H_2L^2 and H_3L^3, and other similar complexes

Complex	g_x	g_y	g_z	μ/λ	R/λ	E_1/λ	R/μ	Ref.
$[FeL^2]^+$	1.733	2.349	2.624	−3.797	1.623	−2.683	−0.428	This work
$[FeL^3]$	1.730	2.354	2.646	−3.784	1.759	−2.676	−0.465	This work
$[FeL^1]^+$	1.721	2.337	2.683	−3.735	1.925	−2.647	−0.515	1
$[Fe(accyclam)]^{2+ a}$	1.910	2.237	2.511	−6.103	3.957	−4.166	−0.648	24
$[Fe(cyclam)Cl_2]^{+ b}$	1.15	2.23	3.26	2.595	1.266	−1.789	0.488	23
$[Fe(cyclam)Br_2]^{+ b}$	1.08	2.34	3.25	2.137	1.272	−1.655	0.595	23
$[Fe(diammac)]^{3+ c}$	1.631	2.463	2.841	−3.033	1.379	−2.214	−0.455	21
$[Fe(phen)_3]^{3+ d}$	1.459	2.615	2.727	−2.484	0.297	−1.883	−0.119	26

$$A = \frac{g_x + g_y - 2g_z}{4\sqrt{(g_x + g_y - g_z)}}, B = \frac{g_x + g_y}{2\sqrt{2}(g_x + g_y - g_z)}, C = \frac{g_y - g_x}{4\sqrt{(g_x + g_y - g_z)}}, \frac{\mu}{\lambda} = \frac{\{-A^2 + B^2 + C^2 + 2^{-\frac{1}{2}}[AB + (BC^2/A)]\}}{\sqrt{2}[-AB + (BC^2/A)]}, \frac{R}{\lambda} = \frac{(2AC + \sqrt{2}BC)}{C^2 - A^2}, \frac{E_1}{\lambda} = \frac{2}{3}(\frac{\mu}{\lambda}) - \frac{A}{\sqrt{2}B}.$$

^{a} accyclam = *N*-Carboxymethyl-1,4,8,11-tetraazacyclotetradecane. ^{b} cyclam = 1,4,8,11-Tetraazacyclotetradecane. ^{c} diammac = 6,13-Dimethyl-1,4,8,11-tetraazacyclotetradecane-6,13-diamine. ^{d} phen = 1,10-Phenanthroline.
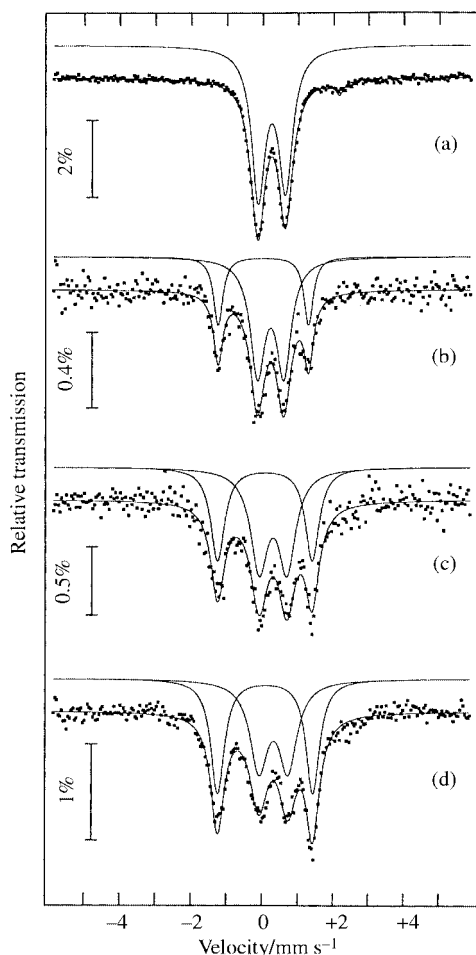

Fig. 10 Mössbauer spectra of (a) $[FeL^3]$ taken at 297 K and of $[FeL^2]^+$ at (b) 297, (c) 150 and (d) 9 K. The lines over the experimental points represent the fits of 2 doublets to each spectrum. The doublets are shown slightly shifted for clarity.

to g_x, g_y and g_z and to determine the sign of each, it is necessary to calculate the values for A, B and C which satisfy the normalisation condition $A^2 + B^2 + C^2 = 1$, and simultaneously give rise to a maximum value for $|\mu/\lambda|$ and a positive value of R/λ. The calculated values for our iron(III) complexes together with those of other similar ones from the literature are collected in Table 7. Both complexes, as well as $[FeL^1]^+$,[1] present moderate to large rhombicity value $|R/\mu|$ (the maximum rhombicity is 0.667)[20] although the lowest value is for $[FeL^2]^+$, followed by that of $[FeL^3]$. Similar EPR parameters and rhombicity values are exhibited by other iron(III) complexes of tetraaza 14-membered macrocycles[21,23–25] and haem derivatives.[19,23] However, the rhombicity value for the complex $[Fe(accyclam)]^{2+}$, a

mono(carboxymethyl) derivative of cyclam (1,4,8,11-tetra-azacyclo-tetradecane) is larger.[24] The EPR parameters of the iron(III) complex with 1,10-phenanthroline are also indicated in Table 7 for comparison, which reveal a much smaller rhombicity value as it is known that axial symmetry is very closely approximated.[26] The value of λ for similar octahedral iron(III) complexes is between −310 and −460 cm^{-1},[21,23] so positive μ values are obtained for all our complexes. Following considerations of Poon and co-workers,[23] positive values of μ imply that the axial ligands are weaker than the equatorial ones and that the d_{xy} orbital is lower in energy than d_{xz} and d_{yz}.

Mössbauer spectra of both $[FeL^2]^+$ and $[FeL^3]$ were fitted by a sum of quadrupole doublets as shown in Fig. 10(a). The width and relative area of both lines in each quadrupole doublet were kept equal during the refinement procedure. The estimated parameters for each doublet (isomer shift, δ, quadrupole doublet, Δ, linewidths, Γ, and relative intensities, I) are summarised in Table 8.

In the sample of $[FeL^3]$ a small amount of an Fe containing impurity was evidenced by a quadrupole doublet with a resolved line at ≥ 2 mm s^{-1}. The presence of this doublet did not affect the analysis of the Mössbauer data. Besides this impurity the spectra of the $[FeL^3]$ sample show a doublet with hyperfine parameters (Table 8) consistent with high-spin Fe^{III} in agreement with the EPR data.

The sample of $[FeL^2]^+$ shows two quadrupole doublets; δ and Δ of one of them are, within experimental error and at all measured temperatures, the same as those estimated for the high-spin Fe^{III} observed in the $[FeL^3]$ spectra. The other quadrupole doublet with a lower δ and a larger Δ suggests the presence of a low-spin iron(III) species.[27–30] Both iron(III) species are present in the studied temperature range from 9 up to 297 K. Assuming that the temperature dependence of the recoil-free fractions of the two species are not very different, the relative areas of the corresponding quadrupole doublets (Fig. 9b and Table 8) indicate that the amount of the high-spin species increases with temperature. This increase is moderate between 9 and 78 K and becomes steeper as the temperature increases.

Molecular mechanics calculations and conclusions

The X-ray determinations of $[ML^1]$ (M = Co^{III} or Ni^{II}), $[CuL^2]$ (ref. 2) and $[ML^3]$ (M = Co^{III} or Cu^{II}) have shown that in the solid state these complexes have a *trans*-octahedral geometry with four nitrogen atoms of the macrocyclic ligand forming the equatorial co-ordination plane. The axial positions in the complexes of H_3L^3 are occupied by two oxygen atoms from the carboxymethyl arms bound to contiguous amines of the macrocycle. By contrast to the complexes of H_2L^1 and H_2L^2, those positions belong naturally to the two oxygen atoms of carboxymethyl arms bound to amines adjacent to the pyridine ring. However, in spite of this structural difference identical conformations were found for the macrocyclic backbone in all

Table 8 Estimated parameters from the Mössbauer spectra of the $[FeL^3]$ and $[FeL^2]^+$ samples taken at different temperatures, T. δ/mm s^{-1}, isomer shift relative to α-Fe at 295 K; Δ/mm s^{-1}, quadrupole splitting; Γ/mm s^{-1}, linewidth; I(%), relative area. Estimated errors ≤ 0.02 mm s^{-1} for δ, Δ, Γ, and $\leq 2\%$ for I. The Fe containing impurity (< 6% of the total Fe) in the $[FeL^3]$ sample is ignored

	$[FeL^3]$ (high spin)			$[FeL^2]^+$ (high spin)				$[FeL^2]^+$ (low spin)			
T	δ	Δ	Γ	δ	Δ	Γ	I	δ	Δ	Γ	I
297	0.36	0.76	0.46	0.34	0.73	0.50	70	0.13	2.53	0.32	30
150	0.44	0.78	0.47	0.43	0.78	0.59	56	0.19	2.66	0.47	44
78	0.47	0.78	0.49	0.46	0.76	0.56	50	0.20	2.64	0.43	50
9	0.47	0.79	0.48	0.45	0.81	0.61	47	0.20	2.67	0.46	53

octahedral metal complexes of those three ligands. These structural features pose the question as to why in the metal complexes of H_3L^3 the carboxymethyl group *trans* to the pyridine ring is used to complete the six-co-ordination instead of the carboxymethyl group adjacent to that ring, as reported for complexes of H_2L^1 or H_2L^2. Furthermore comparison of the structures of the studied complexes with those of $[Cu(H_2-L^1)Cl]^+$ (ref. 12) or $[NiL^4]^{2+}$ (ref. 11) suggests that this type of macrocyclic backbone can adopt easily other different conformations in order to accommodate the metal centre in other geometric arrangements. Indeed, in $[NiL^4]^{2+}$ the metal centre is encapsulated by the macrocyclic ligand in a *cis*-octahedral geometry with two pyridylmethyl groups occupying an axial and equatorial co-ordination positions. The macrocycle is folded along the axis defined by the two nitrogen atoms contiguous to the pyridine ring.

On the other hand the magnetic and spectroscopic studies undertaken with the Fe^{3+} complexes of H_2L^1 and H_2L^2, in solution and in the solid state, have shown the presence of two types of resonances which can be assigned to two isomers in different spin states, a low- and a high-spin species, or can be interpreted by a spin equilibrium between the $S = 5/2$ and $1/2$ states, while the Fe^{3+} complex of H_3L^3 forms only a high-spin species (although a minute amount of a low-spin species in frozen solutions is evidenced by the EPR studies at very low temperature, but not by Mössbauer spectroscopy.). Mössbauer spectroscopy has also revealed that for $[FeL^2]^+$ the amount of the high-spin species increases with temperature being of about 50% at low temperature and of 70% at room temperature. These results also show that the amount of the low-spin species increases smoothly with decrease of temperature ($49 \pm 4\%$ for the range 150 to 9 K). Therefore it is not surprising that the quantitative measurements made by EPR spectroscopy with $[FeL^1]^+$ had shown an almost constant value for the proportion of the low-spin species in the range 9 to 200 K due to the difficulty to quantify the small signals obtained at temperatures higher than 100 K by this technique. The measurement made pointed to a lower percentage of the low-spin species for this complex, $35 \pm 5\%$. A disagreement still persists, for which we do not have an explanation, with the previous temperature-dependent static susceptibility study[1] for $[FeL^1]^+$ which indicated a steep decrease of the magnetic moment value for temperatures below 100 K, exhibiting a value of $1.70\ \mu_B$ at 3.1 K. However in accord with the present work the value of the magnetic moment is almost constant in the region 292 to 100 K ($\mu_{eff} = 3.58\ \mu_B$ at 292 K) which also points to the presence of an equilibrium between low- and high-spin states. The Mössbauer results have also revealed that the high-spin species of the tris- and the bis-(carboxymethyl) derivatives have very similar structures.

Why do the iron(III) complexes of the bis(carboxymethyl) derivatives, H_2L^1 and H_2L^2, exist in an equilibrium between low- and high-spin states while that of the tris(carboxymethyl) one, H_3L^3, practically forms only a high-spin species, when all these ligands form complexes with similar structures with the other metal ions studied? It is known that in general iron(III) complexes with weak-field ligands give high-spin configur-ations and strong-field ligands low-spin ones. Ligands of intermediate strength can form complexes near the crossover point between ^6A and ^2T ground states or exhibit the two spin states simultaneously.[22] Therefore, the iron(III) complex of the tris(carboxymethyl) derivative (H_3L^3) forms a weaker-field complex than one of the isomers of the bis(carboxymethyl) derivatives.

Other cases of equilibrium between $S = 5/2$ and $1/2$ described in the literature for iron(III) complexes have been accompanied by a concomitant structural change. In some cases the octahedral geometry is maintained, but an increase of the Fe–L distances for the high-spin species is observed. However, in other cases the structural change involves a decrease of the co-ordination number from six, for the low-spin, to five for the high-spin species. The average Fe–N$_{amine}$ distances for the octahedral high-spin and low-spin species are about 2.20 and 2.00 Å, respectively.[31–34]

Molecular mechanics (MM) calculations were performed in order to shed some light on the two questions formulated above. As mentioned before three types of geometry, *cis* and *trans* octahedral and trigonal-bipyramidal, have been reported leading to different conformations of the macrocyclic backbone. Therefore, several conformers were taken into account in the MM calculations, which are shown in Fig. 11. For the *trans*-octahedral geometry two different planar arrangements were considered. One similar to the structure determined for the $[ML^1]$ ($M = Co^{3+}$ or Ni^{2+}) and $[CuL^2]$ (*trans b*), and another one where the carboxymethyl groups involved in the co-ordination are those found in the structures of the H_3L^3 complexes, but the free carboxylmethyl was replaced by an isotropic methyl group in order to avoid the problem of the several local energy minima arising from the carboxymethyl group (*trans a*). This designed macrocycle is denoted H_2L^5. The *cis*-octahedral geometry leads to two different isomers for metal complexes of H_2L^1 (*cis b* and *cis c*). In both cases the macrocycle is folded along the line defined by the two nitrogen atoms adjacent to the pyridine ring and the carboxymethyl arms occupy an equatorial and an axial position in the metal co-ordination sphere. The two conformers differ only in the orientation of the methyl group bound to the nitrogen opposite to the pyridine ring. For the *cis*-octahedral arrangement of H_2L^5 only one conformer is possible (*cis a* in Fig. 11). Two five-co-ordinate geometries are also considered in agreement with the experimental structural data found for $[Cu(H_2L^1)Cl]^+$, where the nitrogen *trans* to the pyridine ring stays unco-ordinated and the fifth co-ordination position is occupied by a chloride. In the designed complexes considered the chloride was replaced by a carboxymethyl group and then two extreme geometries for the five-co-ordination arrangements were evaluated, trigonal bipyramidal (TBP) and square planar (SP) as can be seen in Fig. 11.

In Fig. 11 is also included a plot of the steric energy profiles *versus* M–L distances obtained for all the conformers described. The results for the *trans*-octahedral geometries show that for all the range of M–L distances the two curves are superimposed, having a minimum energy at about 2.05 Å. So in the gaseous phase the metal centre can use the carboxymethyl arm *cis* or *trans* to the pyridine ring to achieve the six-co-ordination
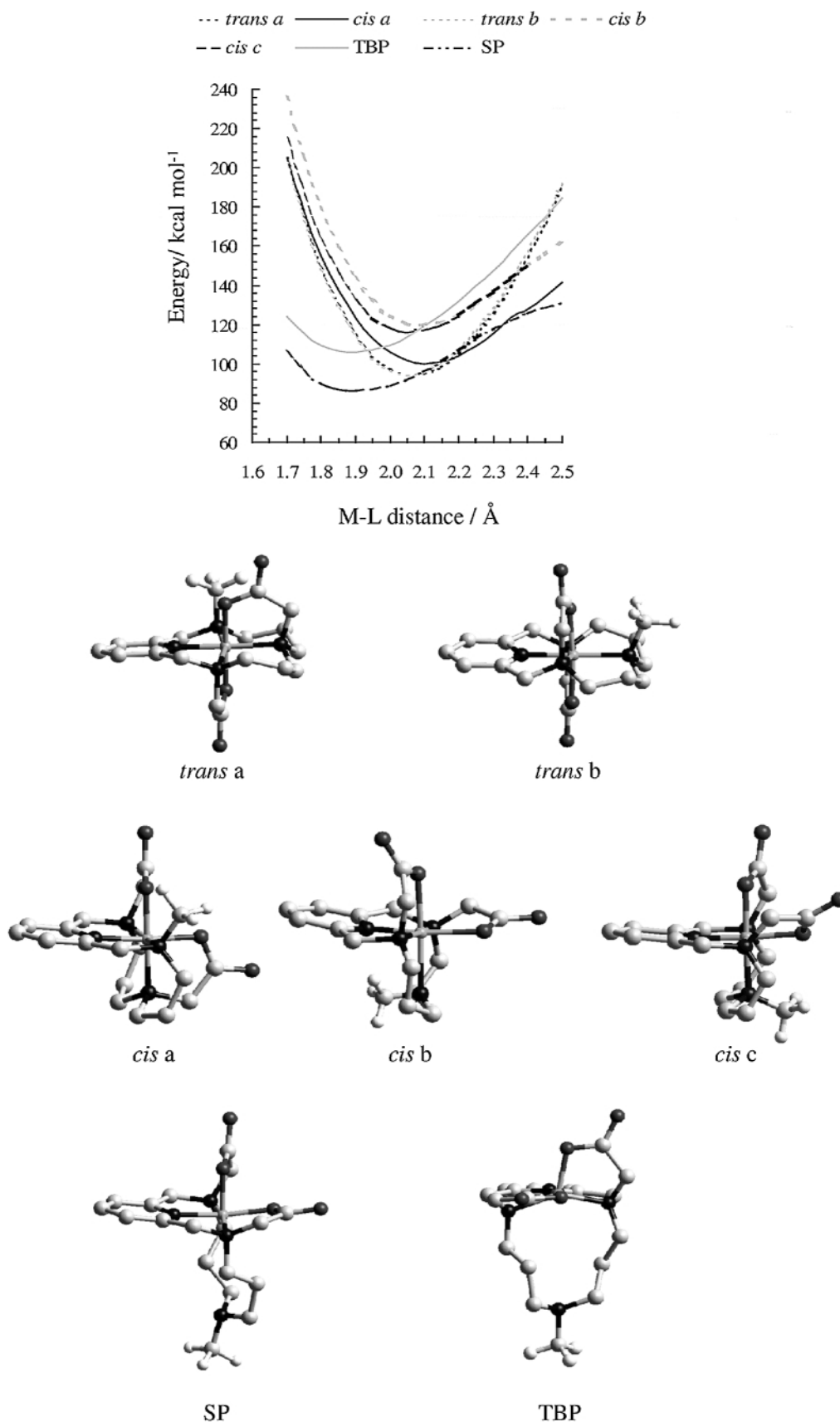
Fig. 11 Steric energy *versus* M–L distance for metal complexes of H_2L^1 and H_2L^5 with sketches of all relevant conformations. For complexes of H_2L^1, square planar (SQ), trigonal bypiramidal (TBP) and *trans*- and *cis*-octahedral geometric arrangements were considered, while for complexes of H_2L^5 only *trans*- and *cis*-octahedral arrangements were taken into account in MM calculations.

geometry. In the studied complexes in the solid state the free carboxymethyl arm adjacent to the pyridine ring is involved in extensive hydrogen-bonding interactions, see above, and therefore are not completely available for co-ordination.

The *cis b* and *c* conformers have higher energy than the *trans* ones up to about 2.35 Å. However the *cis a* conformer has a completely different behaviour exhibiting lower energies than *cis b* and *c* over the range of M–L distances and

becomes more stable than the *trans a* and *b* at distances up to 2.20 Å.

The five-co-ordinate conformers display a striking behaviour showing broad energy profiles with the energy minimum at shorter M–L distances (1.90 Å for TBP and 1.95 Å for SP). Furthermore, the SP conformer is more stable than any others until 2.05 Å, indeed the molecular mechanics results suggest that when the nitrogen *trans* to the pyridine ring stays unco-ordinated the strain in the macrocycle is considerably alleviated, particularly for lower M–L distances. However the Fe^{III}–L bond lengths are incompatible with the M–L distances where these two structures are more stable than the other isomers and therefore will be disregarded in the following discussion.[31–34]

The low-spin species adopted by the iron(III) complexes having stronger ligand field would correspond to the *trans*-octahedral arrangements, while the high-spin species leading to a weaker ligand field likely adopt a folded geometry which leads to longer distances and more strained structures. The molecular mechanics diagram shows that the *cis a* conformer is the preferred structure for M–L distances up to 2.20 Å, which is the average value for the bond distances of the iron(III) complexes in the high-spin state. This conformer corresponds to a possible arrangement of the complexes of H_3L^3 which use the carboxymethyl group bound to the nitrogen opposite to the pyridine ring. However the close position of the minimum energy of the *trans* conformers at lower energies for distances of about 2.00 Å would suggest a spin equilibrium between both conformers. Unfortunately in the MM calculations of the strain energies in Fig. 11 the pairing energy for the low-spin state can not be taken into account. If this additional energy is summed with the steric energy in the diagram both curves corresponding to the *trans* conformers will shift along the *y* axis putting them adjacent to the curves of *cis b* and *c* conformers, suggesting that one of these conformations can be adopted for the high-spin state species with average M–L distances of 2.20 Å. In other words, these results became consistent with the equilibrium between a low-spin species with a *trans*-octahedral geometry and a high-spin species with *cis* octahedral geometry (*cis b* or *c*) for the iron(III) complexes of H_2L^1 or H_2L^2. The mentioned shift of the energy corresponding to the *trans* conformers leaves the curve corresponding to the *cis a* structure, which would be an adopted conformation of the iron(III) complexes of H_3L^3, in the lower position with the minimum at about 2.15 Å, being the predicted structure for the high-spin species consistent with our EPR and Mössbauer spectroscopic experimental data.

Acknowledgements

References

1 J. Costa, R. Delgado, M. C. Figueira, R. T. Henriques and M. Teixeira, *J. Chem. Soc., Dalton Trans.*, 1997, 65.
2 J. Costa, R. Delgado, M. G. B. Drew and V. Félix, *J. Chem. Soc., Dalton Trans.*, 1998, 1063.
3 A. J. Stone, appendix to G. M. Bancroft, A. G. Maddock, W. K. Ong, R. H. Prince and A. J. Stone, *J. Chem. Soc. A*, 1967, 1966.
4 W. Kabasch, *J. Appl. Crystallogr.*, 1988, **21**, 916.
5 N. Walker and D. Stuart, DIFABS, *Acta Crystallogr., Sect. A*, 1983, **39**, 158.
6 G. M. Sheldrick, SHELX 97, University of Göttingen, 1997.
7 L. Zsolnai, XPMA and ZORTEP, University of Heidelberg, 1994.
8 A. L. Spek, PLATON, a Multipurpose Crystallographic Tool, Utrecht University, Utrecht, 1999.
9 CERIUS 2, version 3.5, Molecular Simulations Inc., San Diego, 1997.
10 A. K. Rappé, C. J. Casewit, K. S. Colwell, W. A. Goddard III and W. M. Skiff, *J. Am. Chem. Soc.*, 1992, **114**, 10024.
11 K. P. Balakrishnam, H. A. A. Omar, P. More, N. W. Alcock and G. A. Pike, *J. Chem. Soc., Dalton Trans.*, 1990, 2965.
12 W. Alcock, P. Moore and H. A. A. Omar, *J. Chem. Soc., Chem. Commun.*, 1985, 1058.
13 B. J. Hathaway, *Coord. Chem. Rev.*, 1983, **52**, 87.
14 V. Félix, M. J. Calhorda, J. Costa, R. Delgado, C. Brito, M. T. Duarte, T. Arcos and M. G. B. Drew, *J. Chem. Soc., Dalton Trans.*, 1996, 4543 and refs. therein.
15 A. F Wells, *Structural Inorganic Chemistry*, Clarendon Press, Oxford, 1984, pp. 78 and 79.
16 F. H. Allen, J. E. Davies, J. J. Galloy, O. Johnson, O. Kennard, C. F. Macrae and D. G. Watson, *J. Chem. Inf. Comput. Sci.*, 1991, **31**, 204.
17 W. R. Hagen, in *Adv. in Inorg. Chem.*, 1992, **38**, 165.
18 G. Palmer, in *The Porphyrins*, ed. D. Dolphin, 1979, vol. 4, Academic Press, New York, pp. 313–353.
19 T. L. Bohan, *J. Magn. Reson.*, 1977, **26**, 109.
20 G. Palmer, *Biochem. Soc. Trans.*, 1985, 548.
21 P. V. Bernhardt, P. Comba, T. W. Hambley and G. A. Lawrance, *Inorg. Chem.*, 1991, **30**, 942.
22 P. H. Rieger, *Coord. Chem. Rev.*, 1994, **135/136**, 203.
23 A. Desideri, J. B. Raynor and C.-K. Poon, *J. Chem. Soc., Dalton Trans.*, 1977, 2051.
24 W. S. Szulbinski and D. H. Busch, *Inorg. Chim. Acta*, 1995, **234**, 143.
25 N. F. Curtis, L. Xin and D. C. Weatherburn, *Inorg. Chem.*, 1983, **32**, 5838.
26 J. Baker, L. M. Engelhardt, B. N. Figgis and A. H. White, *J. Chem. Soc., Dalton Trans.*, 1975, 530.
27 A. Malliaris and V. Papaefthimiou, *Inorg. Chem.*, 1982, **21**, 770.
28 S. Koch, R. H. Holm and R. B. Frankel, *J. Am. Chem. Soc.*, 1975, **97**, 6714.
29 H.-J. Küppers, K. Wieghardt, B. Nuber, J. Weiss, E. Bill and A. X. Trautwein, *Inorg. Chem.*, 1987, **26**, 3762.
30 W. O. Koch, V. Schünemann and M.-J. Krüger, *Chem. Eur. J.*, 1998, **4**, 1255.
31 S. Hayami, T. Matoba, S. Nomiyama, T. Kojima, S. Osaki and Y. Maeda, *Bull. Chem. Soc. Jpn.*, 1997, **70**, 3001.
32 W. O. Koch, V. Schünemann, M. Gerdan, A. X. Trautwein and H.-J. Krüger, *Chem. Eur. J.*, 1998, **4**, 686.
33 W. R. Scheidt and C.A. Reed, *Chem. Rev.*, 1981, **81**, 543.
34 P. G. Sim, E. Sinn, R. H. Petty, C. L. Merrill and L. J. Wilson, *Inorg. Chem.*, 1981, **20**, 1213.